GEODYNAMICS & TECTONOPHYSICS
Published by the Institute of the Earth's Crust, Siberian Branch, Russian Academy of Sciences

PALEOGEODYNAMICS

2023 VOLUME 14 ISSUE 2 ARTICLE 0691

ISSN 2078-502X

DOI: 10.5800/GT-2023-14-2-0691

PETROCHEMICAL AND STRUCTURAL CHARACTERISTICS OF PORPHYRY COPPER MINERALIZATION IN THE ASTANEH ORE DEPOSIT, MIDDLE PART OF THE URUMIEH-DOKHTAR MAGMATIC ARC (IRAN)

S. Beygi [1]✉, **M. Tadayon** [1], **R.K. Ilalova** [1], **I.V. Talovina** [1], **T.C. Meisel** [3]

[1] Saint Petersburg Mining University, 2 21st Line, Saint Petersburg 199106, Russia
[2] University of Isfahan, Azadi Sq, Isfahan 8174673441, Iran
[3] Montanuniversität Leoben, 18 Franz-Josef-Straße, Leoben A-8700, Austria

ABSTRACT. Within the Urumieh-Dokhtar Magmatic Arc in the central part of Iran, the formation of which is associated with the Neotethys closure, there are many porphyry copper deposits and ore occurrences. One of them is the Astaneh porphyry copper ore deposit, located in the central part of the Saveh-Ardestan ore region southeast of Ardestan city. The purpose of this study is to investigate the petrochemical characteristics of rocks and to determine the relationship between the distribution of porphyry copper mineralization and tectonic position of faults within the study area. To achieve the goal, there were used the structural and geological data obtained in the fieldwork, as well as the results of mineralogical and geochemical analyses. The obtained results show that rocks of different composition of the Astaneh ore deposit (andesite, andesite-basalt, basalt, trachybasalt) were formed in the suprasubduction zone, and probably in the environment prior to the collision of the of continental plates. Paragenetic relationships and mineralogical analysis show that the evolution of mineralization of the Astaneh ore deposit can be divided into three stages: pre-ore, hypogene and supergene mineralization. Geochemical research based on the study of the content of the major chemical elements in the rocks of the region shows that igneous rocks belong to calc-alkaline basalts and geodynamically can be attributed to the products of magmatism of the ensial island arc. The results concluded that the main stages of the formation of a porphyry copper ore deposit in the study area attain maximum spatio-temporal similarity with the tectonomagmatic phases of the development of the Neotethys Ocean. In addition, the Southern Ardestan fault, running through the study area and intersecting the basement structures, forms wide permeable zones favorable for the formation of porphyry copper deposits therein.

KEYWORDS: porphyry copper mineralization; South Ardestan fault; Urumieh-Dokhtar Magmatic Arc; Astaneh ore deposits; Neotethys Ocean

FUNDING: Not specified.

RESEARCH ARTICLE

Correspondence: Soheyla Beygi, beygi.soheyla@yahoo.com

Received: June 24, 2022
Revised: September 29, 2022
Accepted: October 13, 2022

FOR CITATION: Beygi S., Tadayon M., Ilalova R.K., Talovina I.V., Meisel T.C., 2023. Petrochemical and Structural Characteristics of Porphyry Copper Mineralization in the Astaneh Ore Deposit, Middle Part of the Urumieh-Dokhtar Magmatic Arc (Iran). Geodynamics & Tectonophysics 14 (2), 0691. doi:10.5800/GT-2023-14-2-0691

1. INTRODUCTION

In Iran, there is one of the world's largest porphyry copper belt which was formed for a long period of time from the Late Eocene (39 Ma) to the Late Miocene (6.19 Ma). Most of the porphyry copper and epithermal deposits in Iran were formed within the Urumieh-Dokhtar Magmatic Arc (UDMA) during the closure of the Neothetys Ocean [Shahabpour, 2005; Afzal et al., 2012; Aghazadeh et al., 2015; Richards, Sholeh, 2016] (Fig. 1, a). The porphyry copper deposits and ore occurrences within UDMA are mainly found in three areas which include Kerman in the southeast, Saveh-Ardestan in the central UDMA, and Arasbaran in the northwest [Zarasvandi et al., 2005] (Fig. 1, a). The published results of the Saveh-Ardestan ore deposits in the central UDMA suggest that the mineralization occurred in the period from 17 to 15 Ma which corresponds to the Middle Miocene [Richards et al., 2012; Aghazadeh et al., 2015].

The structural-tectonic control of mineralization within the Urumieh-Dokhtar Magmatic Arc was studied by many researchers. In 1985, M. Nogol-Sadat [Nogol-Sadat, 1985] first investigated the tectonic position of transpressive structures of the Urumieh-Dokhtar Magmatic Arc. In 1991, M. Alavi [Alavi, 1991] determined that the NW-striking Urumieh-Dokhtar Magmatic Arc was displaced repeatedly by the NNW-striking tectonic faults. A study in the petrology of the Urumieh-Dokhtar Magmatic Arc was carried out by [Aftabi, Atapour, 2000].

In succeeding years, M. Aghazadeh et al. [Aghazadeh et al., 2015] studied spatiotemporal distribution and tectonic confines of the porphyry copper deposits in Iran. The multiple subsequent detailed studies in the Ardestan area were made on the composition of intrusive rocks [Babazadeh et al., 2017; Alaminia et al., 2020]. Besides, the study of tectonic structure, mineralogy and regularities in the distribution of these ore deposits was dealt with in the publications of Russian and other foreign researchers [Arshamov, 2013; Krivtsov, 1983; Krivtsov et al., 1986; Parfenov et al., 2003; Richards, 2005; Sillitoe, 2010; и др.].

This paper deals with the study of the Astaneh ore deposit in the central UDMA (Fig. 1, a, b). No geological survey of this porphyry copper deposit has been made yet. The authors of this paper obtained new results on genetic and spatial relationships between mineral distribution, geochemical composition, hydrothermal changes and structural localization of ore zones. The main objectives of this study are:

1) geochemical and mineralogical-petrographical analyses of the rocks in the investigated area;

2) determination of paragenetic types of minerals;

3) determination of the relationship between the distribution of porphyry copper deposits, their geochemical characteristics and orientation of faults. Generalizing study results will be further involved in consideration of ore-forming metallogenic processes and genetic modeling of the porphyry copper mineralization occurrence within UDMA.

2. GEOLOGY OF THE URUMIEH–DOKHTAR MAGMATIC ARC

The formation of the Urumieh-Dokhtar Magmatic Arc (UDMA) is related to the Middle-Late Mesozoic to the Middle Paleogene subduction of the Neotethys oceanic crust beneath the central Iranian plate. The magmatic arc consists of extensive volcanic units with small intrusive bodies emerged along the southern margin of the Iranian Plate [Berberian F., Berberian M., 1981; Richards, 2005; Sillitoe, 2010; Chiu et al., 2017]. The UDMA activity occurred in three temporal stages: Eocene, Oligocene-Miocene and Pliocene-Quaternary [Sayari et al., 2015]. Eocene magmatism in the UDMA includes volcanogenic and volcanogenic-sedimentary rocks such as andesites, basalts, dacites, rhyodacites, rhyolites, and calc-alkaline pyroclastic rocks which occurred on the active continental margins due to the oceanic plate subduction [Atapour, Aftabi, 2007; Shafiei et al., 2009]. The peak of volcanic activity was in the Eocene, with the earliest known structures assigned to the Early Eocene (Ypresian, 55–50 Ma; [Shahabpour, 2005]). The Oligocene-Miocene magmatic activity took place at the late stages of the evolution of the Neotethys – during the continental collision of the Arabian Plate with the Central Iran Microcontinent. Most of the faults within UDMA have NW strike and are one of the factors controlling its magmatic activity. It started from the Late Oligocene lava flows and ended with the Miocene volcanic and intrusive activities [Sayari et al., 2015]. Mineral composition of this magmatic phase changes from one part to another. Intrusive bodies of the magmatic arc usually have porphyritic structure and are composed of intermediate and acid rocks – from diorite to quartz diorite, granodiorite and sometimes quartz monzonite. These rocks are rich in alumina and related to the magnetite-series (I) granitoids [Sarjoughian, Kananian, 2017]. The Pliocene-Quaternary magmatic bodies represent the last phase of magmatic activity and form the basalt, andesite and alkali-trachyte lava sheets overlying the sedimentary deposits [Allen et al., 2004]. This magmatic activity is assigned to the post-collisional stage of the territorial formation which is related to the crustal deformation and uplift caused by orogeny [Allen et al., 2004; Ageev et al., 2020].

3. GEOLOGY OF THE ASTANEH ORE DEPOSIT

The Astaneh area is located southwest of Ardestan City, with several porphyry copper deposits and ore occurrences in the Oligocene-Miocene rocks therein (Fig. 1, b; 2, a). Geology of the Astaneh area is characterized by the Eocene and Miocene magmatic rocks and small separate Miocene sediment residuals. The oldest rocks – Eocene andesites, andesibasalts, tuff breccias and ignimbrites – are bordering the south and the west of the study area (Fig. 2, a). The Oligocene-Miocene andesitic basalt lavas and their altered varieties are located in the central part of the area.

On the southeast and south, the Astaneh ore deposit is bounded by disjunctive structures: right-lateral transpressive South Ardestan fault and Kacho-Mesghal fault (see

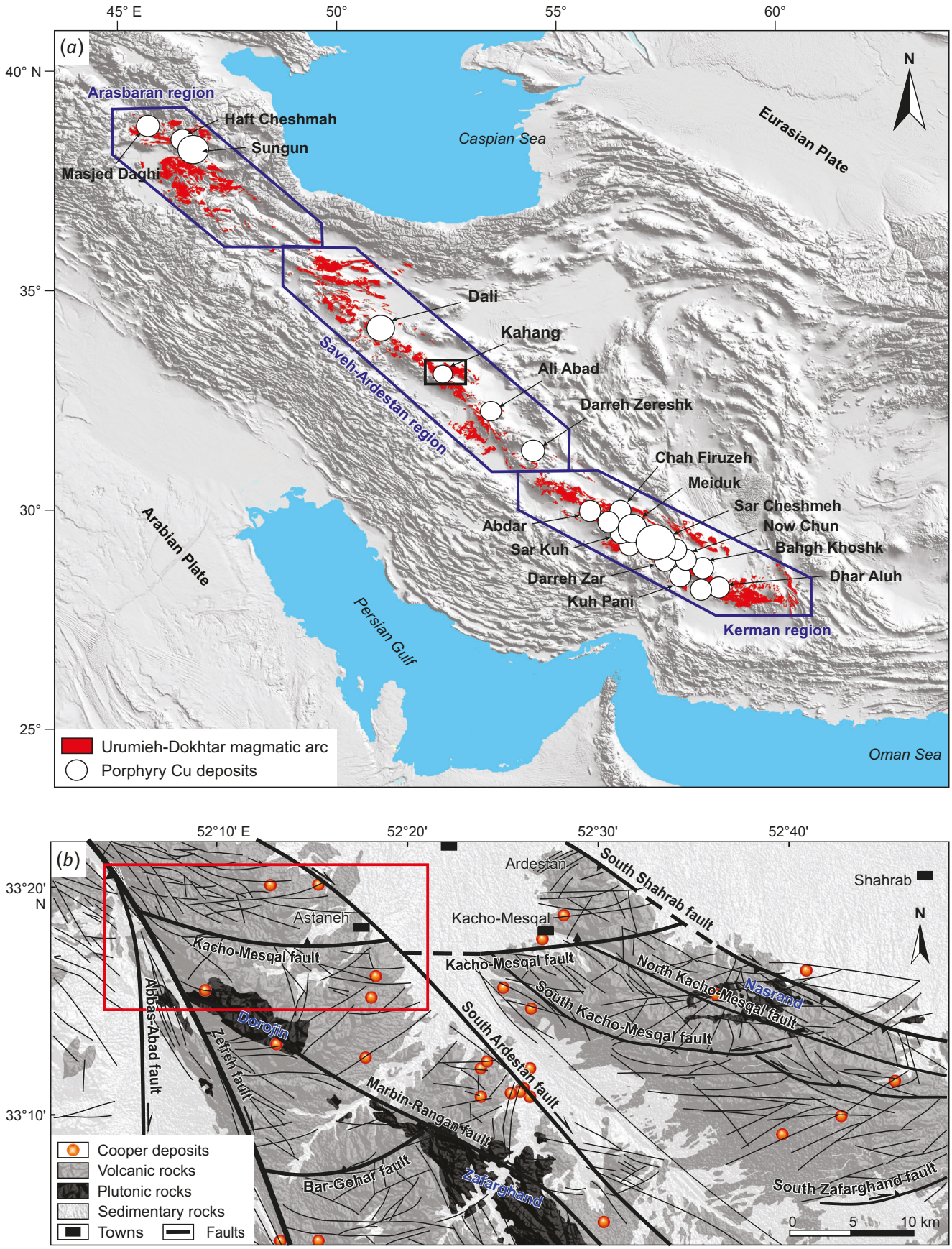

Fig. 1. Location of the study area.
(*a*) – a shaded topographic relief map of Iran showing the location of the main porphyry copper deposits; (*b*) – a map of the distribution of volcanic and plutonic rocks in the central part of the Urumieh-Dokhtar Magmatic Arc (UDMA). The red rectangle marks the study area.

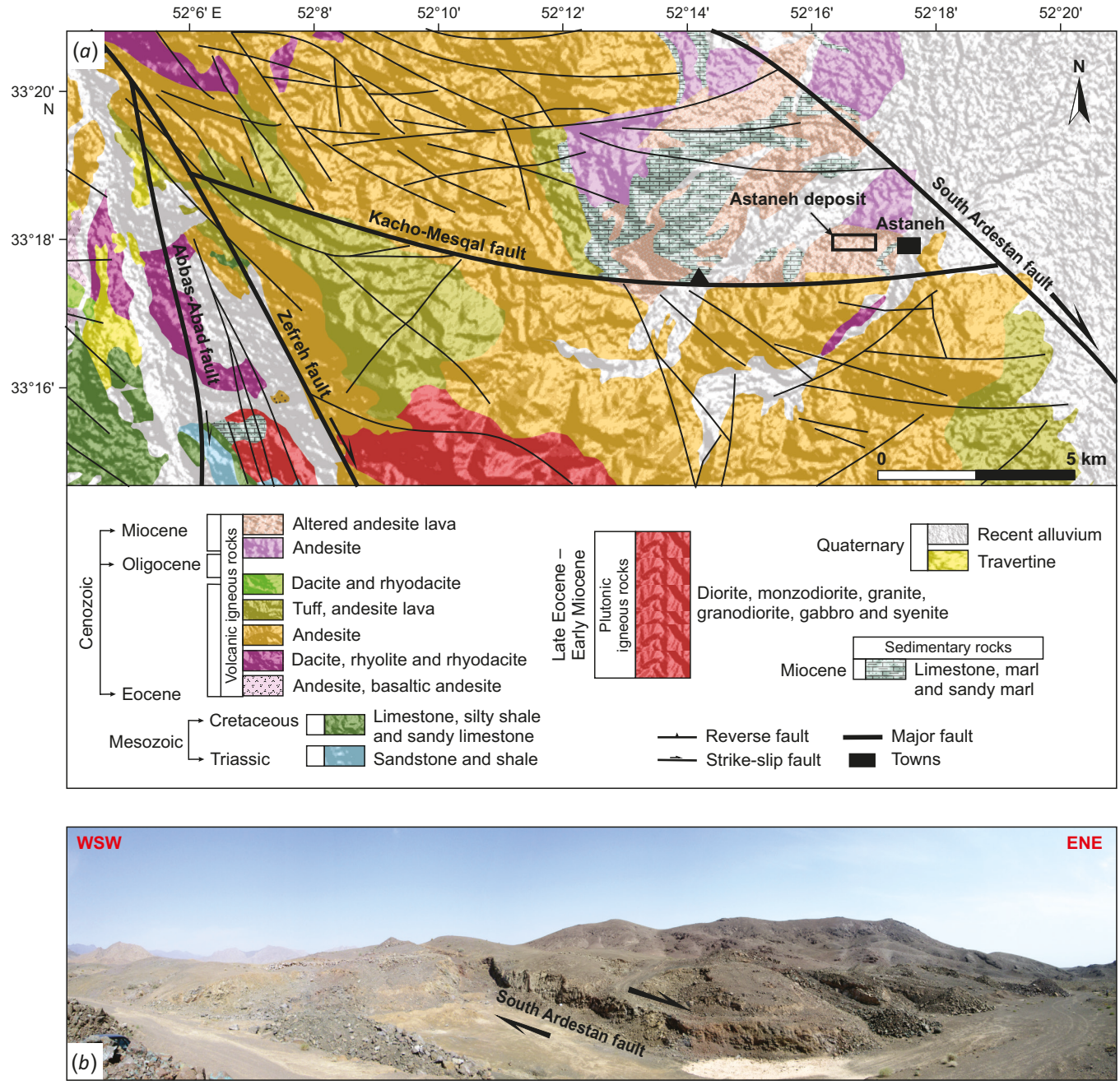

Fig. 2. Rock units in the study area.
(*a*) – a geological map of the study area showing the main tectonic structures; (*b*) – location of the Astaneh ore deposit in the Oligocene-Miocene andesites and andesibasalts.

Fig. 1, b; Fig. 2, a), in their turn complicated and deformed by subparallel and transverse tectonic faults. The South Ardestan fault is about 120 km long and borders the west of the Ardestan depression (see Fig. 1, b; Fig. 2, a). Field observations and interpretation of satellite images show that the fault has a strike azimuth of 300–310° [Beygi et al., 2016, 2018a, 2018b, 2021a]. The active Kacho-Mesghal fault with reverse kinematics intersects the Miocene andesite lavas and Eocene andesites near Astaneh village. In the west, this structure adjoins the Zefreh fault (see Fig. 1, b; Fig. 2, a) which changes its strike azimuth [Beygi et al., 2016, 2018a, 2018b, 2021b].

4. MATERIALS AND METHODS

The study area is located west of Astaneh village in the Saveh-Ardestan ore region (Fig. 2, a, b). For its geological mapping, there were selected 45 hand specimens from hydrothermal-metasomatic rock outcrops along the South Ardestan fault zone. Based on the field observation results, there were specified the boundaries of the distribution of magmatic bodies and the features of their structural relationship with the South Ardestan fault plane.

The field investigations of fault structures involved the study of strike azimuths and dip angles of fault planes, slickensides and slickenlines. The fault displacement amplitudes

were obtained from the analysis of slickenlines and from the displacement of layers along the fault planes. The strike and dip of the faults obtained from the slickenlines were used for determination of the tectonic stress field pattern. The ratios of the main-compression to main-extension vectors were calculated using Daisy 5.38 (Structural Data Integrated System Analyzer) [Salvini, 1998].

Mineralogical and petrographic composition of the rocks was determined based on 35 transparent and 45 polished thin sections. The results of optical microscopic study in combination with the field observations were used to interpret the rock formation processes and to investigate their ore specialization. During X-ray fluorescence analysis of rocks in trenches, there were selected 45 rock and ore specimens of different composition. The data obtained were then interpreted in Excel using geochemical diagrams and mathematical methods of statistics.

5. DISCUSSION OF RESULTS

5.1. Characteristics of the rocks

The field and laboratory-analytical research on the Astaneh ore deposit shows that it contains andesibasalts, andesites and basalts, of which the most abundant are andesibasalts. The structures of these volcanogenic rocks are mainly porphyritic with microlithic matrix, glomerophyric or hyalomicrolitic. The textures are fluidal and amygdaloidal.

Andesites are composed of andesine, other plagioclases, pyroxene and hornblende; among the secondary minerals are quartz, calcite, chlorite, and iron oxides. Plagioclase, the most common mineral phenocryst in andesites of the Astaneh ore deposit, occurs in the form of idiomorphic or hypidiomorphic grains with polysynthetic twinning, sometimes with lattice texture implying chemical imbalance. Pyroxenes in the andesites are represented by highly fractured augite occurring in two forms – phenocrystal and microphenocrystal, idiomorphic and hypidiomorphic, respectively. Hornblende occurs in the form of small grains, less often – in the form of phenocrysts. Most of the andesites have porphyritic or fluidal textures. The breccia textures are usually restricted to secondary minerals, mainly to quartz. Propylitic alternation is indicated by the presence of quartz, chlorite and pyrite in a rock. Pyrite is oxidized to iron oxides, and chlorite develops after hornblende and plagioclase (Fig. 3, a).

Basalts are rocks dark-gray to black in color, with large amounts of cavities and voids. These cavities are filled with hydrothermal minerals such as malachite, calcite, chlorite and quartz which give the rocks an amygdaloidal texture. Plagioclase, olivine and pyroxene are basic mineral phenocrysts in the basalts studied. Plagioclases in the form of simple and polysynthetic twins are characterized by irregularity of zonal distribution which provides uneven rims and lattice texture. Olivine is found in basalts in the form of large idiomorphic crystals and microcrystals, often replaced entirely by chlorite, calcite and sometimes by iddingsite. Cracks in olivine are filled with iron oxides. Monocline pyroxenes are represented by hypidiomorphic, fine-sized grains of augite in the groundmass of basalt. The basalt structure is predominantly porphyry and porphyry microlithic (Fig. 3 b, c).

Andesibasalts are composed of plagioclase, olivine, pyroxene, and hornblende Secondary minerals within the cavities in rocks sampled are represented by quartz, calcite,

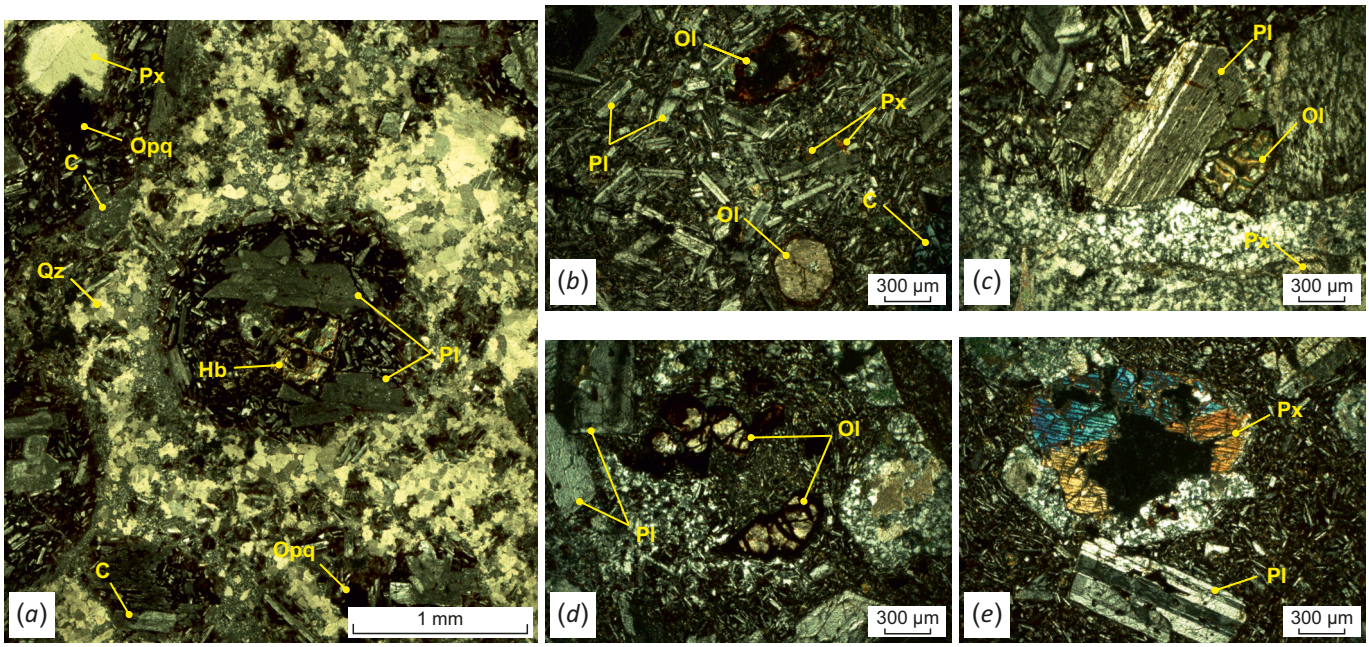

Fig. 3. Microphotographs of the studied volcanic rocks.
(*a*) – andesite (pyroxene + hornblende + plagioclase + quartz + chlorite + opaque mineral); (*b*, *c*) – basalt (olivine + pyroxene + plagioclase + chlorite); (*d*, *e*) – andesibasalts (olivine + pyroxene + plagioclase + chlorite), where Px is pyroxene, Ol – olivine, Opq – opaque mineral, Pl – plagioclase, Hb – hornblende, Qz – quartz, C – chlorite.

chlorite, and iron oxide. Phenocrysts of plagioclase occur as hypidiomorphic or idiomorphic grains, which show twinning in accordance with carlsbad, albite and pericline laws. Olivine phenocrysts are found in andesibasalts in the form of large- and middle-seized idiomorphic grains. Olivine in all samples is replaced by iddingsite, less often by calcite and iron oxide along its rims and fractures. Clinopyroxene occurs in matrix and as idiomorphic to hypidiomorphic phenocrysts. There are found both colorless and colored varieties of the mineral. Idiomorphic to hypidiomorphic hornblende grains in many samples are replaced entirely by opacite or hematite. The dominant textures in these samples are porphyry, porphyry microlithic, with the existing fluidal and almond-shaped textures (Fig. 3, d, e).

5.2. Structural control

The Astaneh ore deposit is structurally located in the zone of dynamic influence of tectonic suture of the South Ardestan disjunctive having the right-lateral strike-slip fault kinematics as noted above (see Fig. 2, b). During the structural observations, there were made measurements of spatial parameters and geometric sampling for 212 faults. Stereographic projections of the data are plotted in Fig. 4 showing the strike and dip directions of faults, presence of slickenlines etc. Among the faults measured, 116 faults have the right-lateral strike-slip kinematics, and 96 – the left-lateral strike-slip fault kinematics (Fig. 4, b, c).

Fig. 4, b, show that most of the right-lateral strike-slip faults are striking northwest (less often northeast), and most of the left-lateral strike-slip faults have east-northeastern strike. The angle of intersection between the faults is close to 90°. Therefore, according to M.V. Gzovsky's method [Gzovsky, 1975], they would be conjugated, i.e. coeval, formed in the tectonic field of submeridional transpression close to the tangential compression. The NW faults are usually much more steeply inclined, from about 75° to 80°, distinctly associated with strike-slip kinematics, whereas the NE-striking systems are more gently sloping, from about 45° to 70°, and have an oblique-slip component. Most of the rare sub-latitudinal faults are gently sloping, from 20° to 40°, and distinctly associated with reverse kinematics.

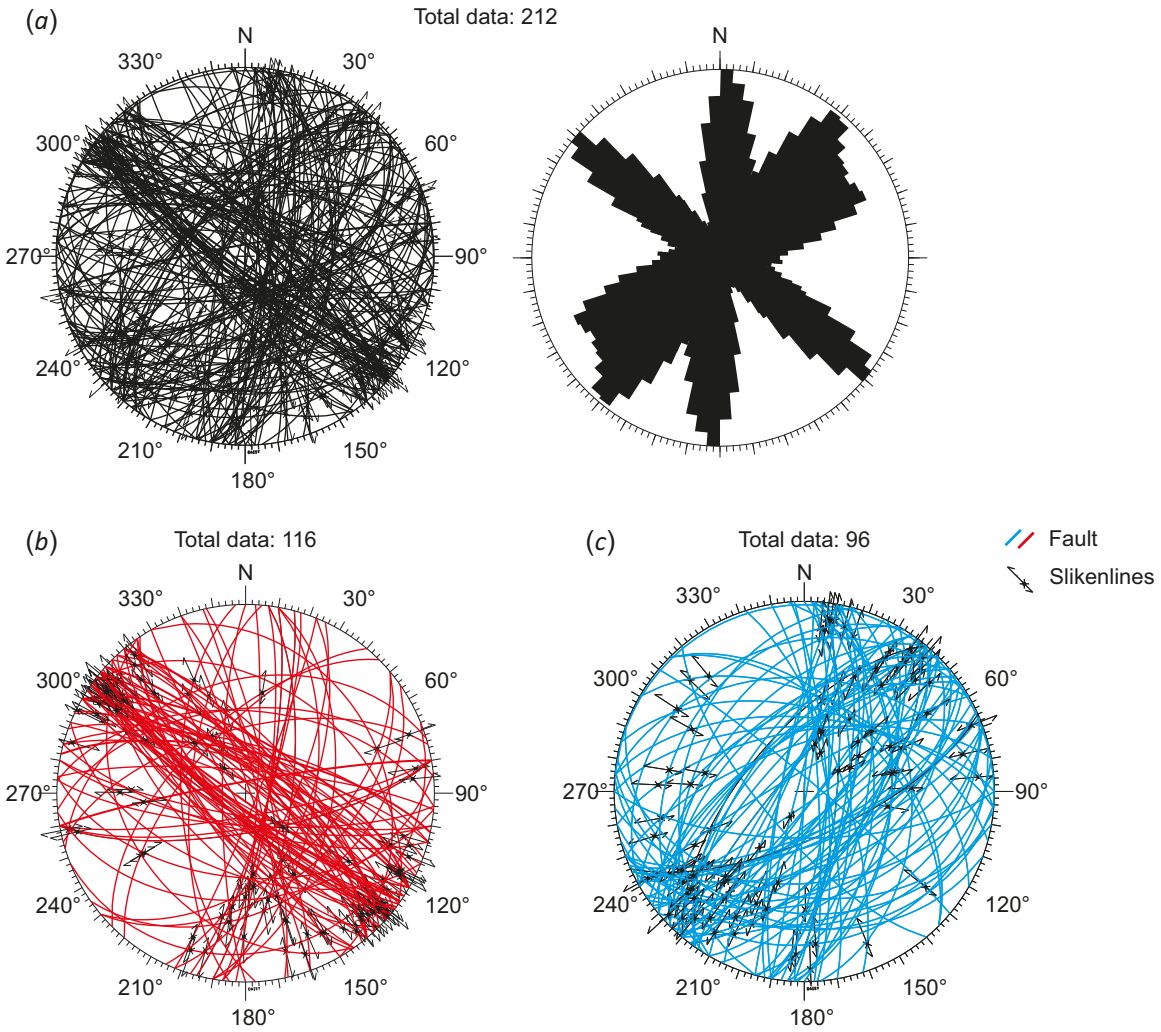

Fig. 4. Stereographic projections measured in the study area.
(*a*) – stereographic projections and rose diagrams of the faults measured; (*b*) – stereographic projections of the right-lateral faults measured; (*c*) – stereographic projections of the left-lateral faults measured.

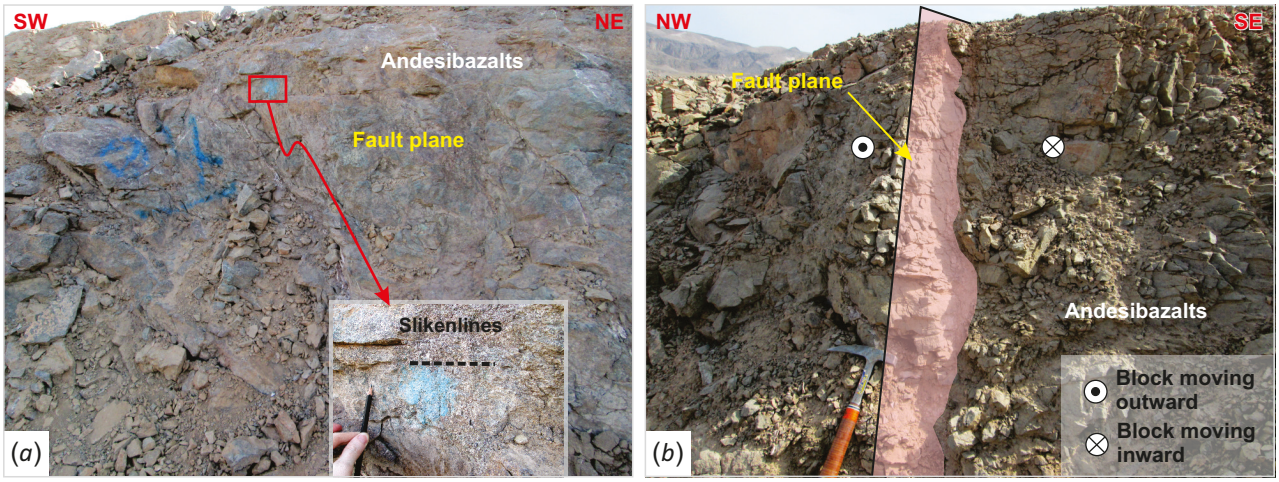

Fig. 5. Fault trace in the field photographs.
(*a*) – South Ardestan fault zone in the Oligocene-Miocene andesibasalts; (*b*) – fault plane in the Oligocene-Miocene andesibasalts with dip azimuth 130° SE and dip angle 65°.

The rocks along the South Ardestan fault generally contain minerals of the propylite association: secondary epidote, albite, quartz ± chlorite ± (barite, malachite, azurite and manganese minerals) (Fig. 5 a, b). This set of minerals usually marks the contours of fault zones and fault planes with tectonic mirrors thereon.

Fig. 5, b demonstrates the fault zone with dip azimuth 130° SE and dip angle 65°. The early left-lateral strike-slip fault and late normal fault kinematics was determined from the two-type slickenline directions (Fig. 5, b).

5.3. Geochemical characteristics

During the study of rocks within the Astaneh ore deposit, chemical analysis was made on 45 samples with trachybasalt), and there were calculated the microelement ratios. For geochemical interpretation and petrological classification by volatile content, oxide factors were used to normalize basic elements to 100 %. SiO_2 content in andesitic basalt samples varies from 52.06 to 54.14 wt. % (52.98 wt. % in the average), in basalt and trachybasalt samples – from 48.39 to 51.79 wt. % (49.94 wt. % in the average), and in andesite samples – from 58.89 to 61.18 wt. % (60.04 wt. % in the average) (Fig. 6, a). The samples whose average total content of alkalis K_2O+Na_2O varies from 3.64 to 5.28 wt. % are plotted in different sections from alkaline-calcium to slightly alkaline rock varieties (Fig. 6, b).

Sr/Y vs. Y diagram is the most widely used discrimination diagram for adakite [Hansen et al., 2002]. The samples studied usually fall within the classical island arc rocks (i.e. relate to normal andesite-dacite-rhyolites) (Fig. 6, c). Relatively low Sr/Y ratios in the rocks (mainly <40) are typical of normal island arc rocks.

Incompatible rare elements and their ratios are typomorphic parameters for determining the hydrodynamic setting during eruption of basaltic magmas. On Sr/Y vs. Zr tectonic discrimination diagram for volcanic rocks [Pearce, 1983], most of the analyzed samples are plotted in the continental arc area (Fig. 6, d).

5.4. Hydrothermal alternation

Hydrothermal alternation of rocks of the Astaneh ore deposit consists of propylitization and argillization. Goethite, hematite, limonite, malachite and azurite are the most widespread secondary minerals of the rocks formed due to the oxidation of sulfide minerals. Propylitic alternation occurs both on the exposed surface and in the rock mass. The minerals that form during propylitic alternation are quartz, chlorite and epidote in combination with negligible amounts of potassium feldspar, plagioclase, sericite, and calcite (Fig. 7, a, b). Epidote occurs as radial, aggregate or patchy replacements of plagioclase phenocrysts (Fig. 7, b). The observation point in Fig. 7, c, is located in the place of occurrence of altered andesite rocks whose reworking is evidenced by the presence of kaolinite and malachite. These minerals develop after andesites and are the indicators of argillitization zones.

6. ORE MINERALIZATION STAGES

The highest-grade ore deposits in the study area are related to the Oligocene-Miocene igneous magmatism. The most important ore minerals therein are pyrite, chalcopyrite, chalcocite, bornite, native copper, covellite, malachite, and azurite (Fig. 8). Besides these minerals, there were observed some amounts of magnetite, hematite, and goethite (Fig. 8). Based on the results of the laboratory studies, there can be distinguished three mineral formation stages: pre-ore, hypogene (major mineralization stage), and supergene post-ore.

Pre-ore mineralization. At the pre-ore stage related to the Neothetys subduction, there occurs a formation of volcanogenic-sedimentary, pyroclastic and volcanic rocks in the region. During primary diagenesis, in the rock mass there is a dispersed granulation of globular pyrite grains (Table 1). There is also an abundance of primarily oxidized magnetite in the ore zone and host rocks. As a result of the secondary processes, the rims of some magnetite grains were replaced by hematite and martite rims (Fig. 8).

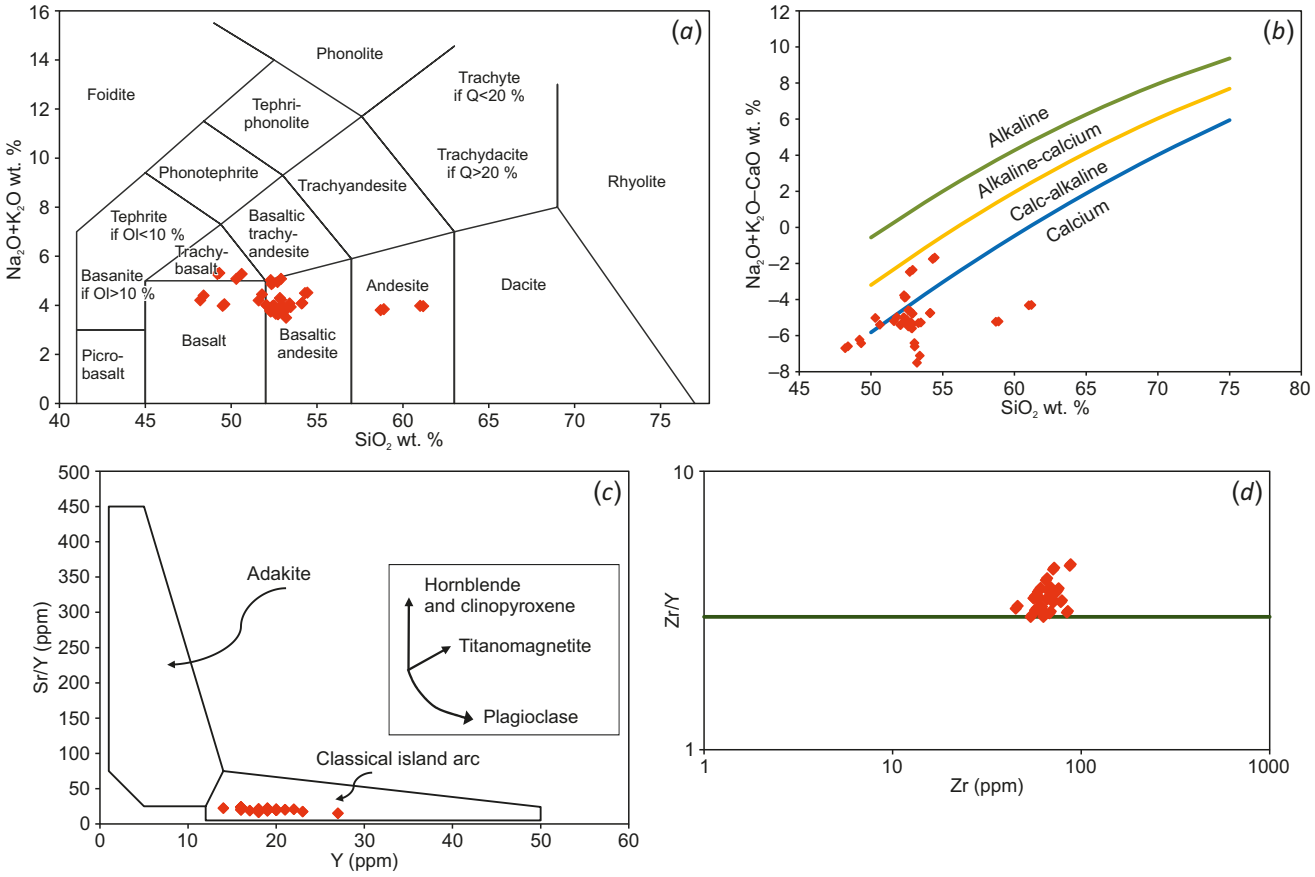

Fig. 6. Geochemical diagram of igneous rocks in the study area.
(*a*) – total alkali vs. silica diagram (TAS) [Le Bas, Streckeisen, 1991]; (*b*) – diagram of Na_2O+K_2O–CaO vs. SiO_2 showing boundaries between the series of alkaline, alkaline-calcium, calc-alkaline and calcium rocks [Frost B.R., Frost C.D., 2008]; (*c*) – volcanic rocks of the Astaneh area, plotted on Sr/Y vs. Y diagram, are divided into adakite and normal andesite-dacite-rhyolite [Hansen et al., 2002]; (*d*) – tectonic discrimination diagram of volcanic rocks in the study area: Zr/Y vs. Zr diagram showing the boundary between the continental and oceanic arcs [Pearce, 1983].

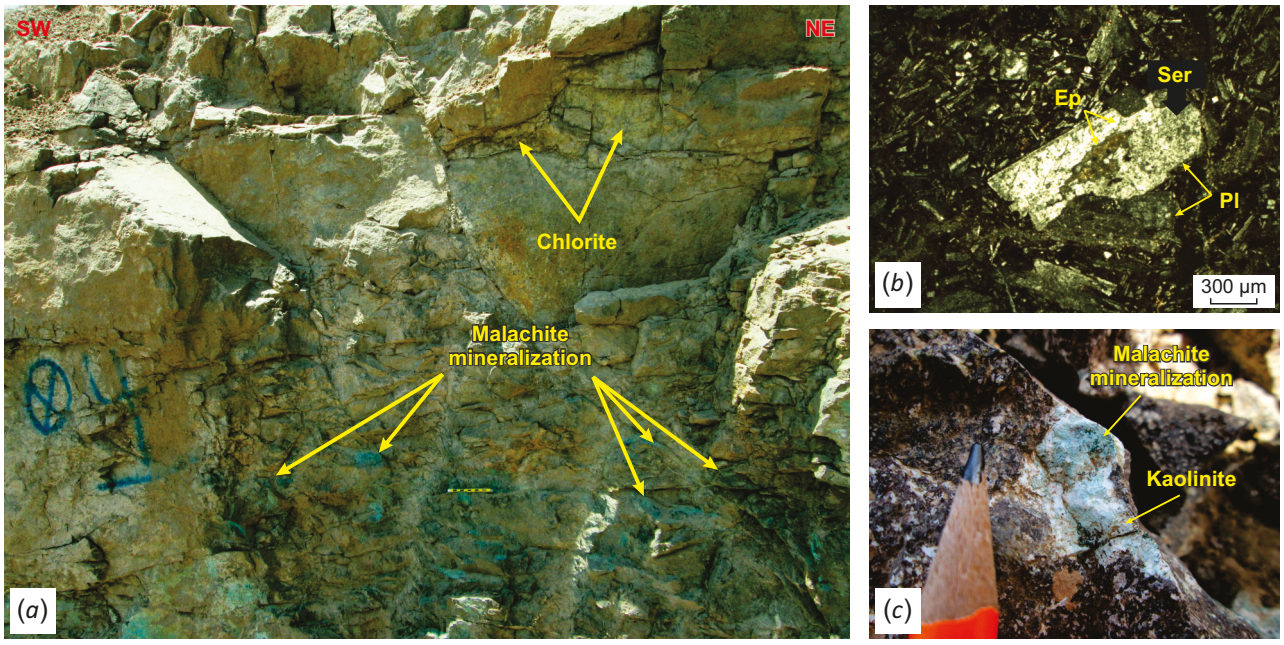

Fig. 7. Microphotographs of the forms of ore mineral in the study area.
(*a*, *c*) – field photographs of the mineralized outcrop the composition of zones of hydrothermal alteration of the rocks; (*b*) – a photograph of thin sections: Ep – epidote, Pl – plagioclase, Ser – sericite.

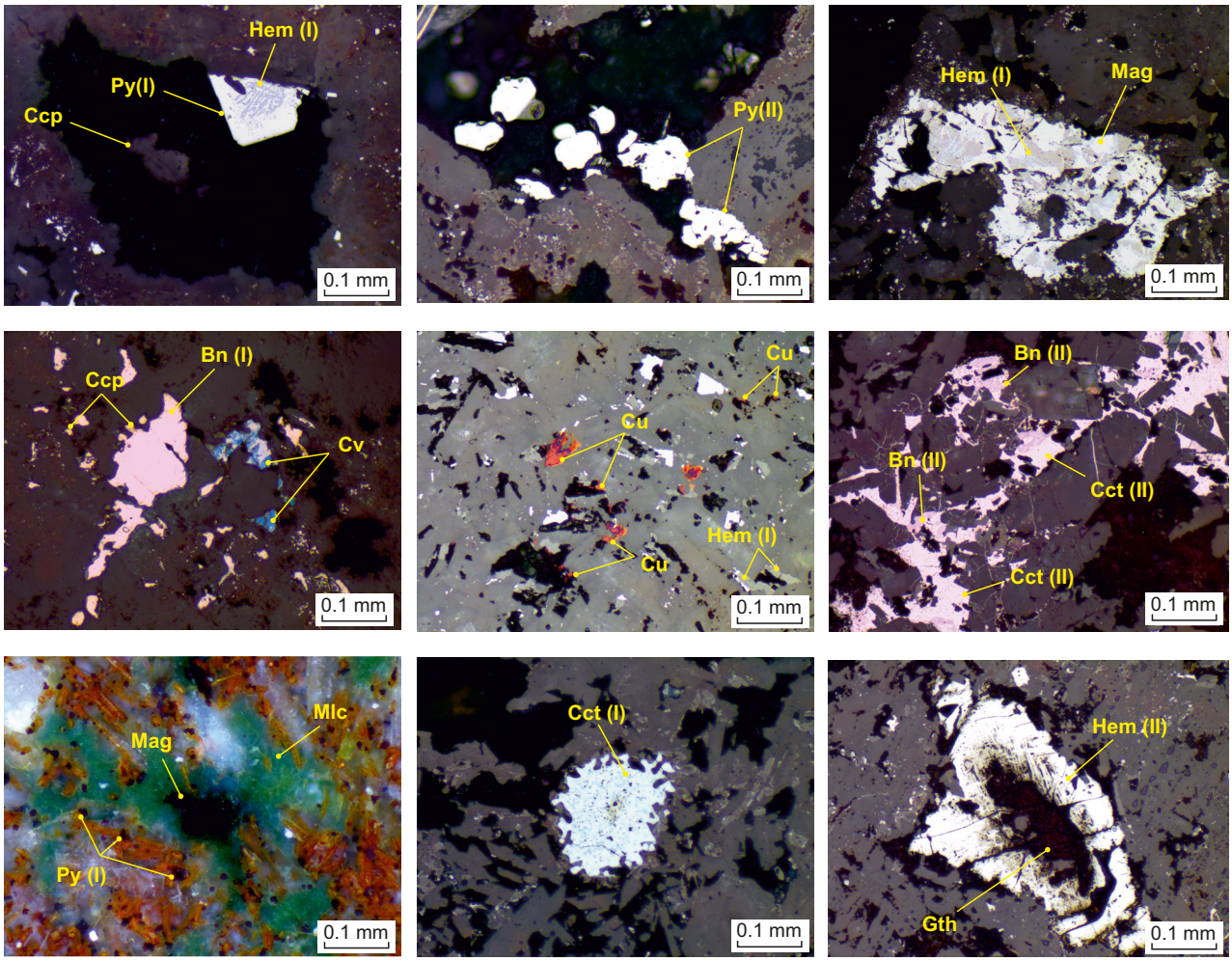

Fig. 8. Microphotographs of ore minerals in the rocks of the Astaneh ore deposit area.
Py – pyrite, Mag – magnetite, Hem – hematite, Gth – goetite, Ccp – chalcopyrite, Cct – chalcocite, Bn – bornite, Cv – covellite, Cu – native copper, Mlc – malachite. I – first-generation minerals, II – second-generation minerals.

Hypogene mineralization. At the major stage of hypogene mineralization, there is a continuation of volcanic activity which leads to a significant increase in volcanogenic-sedimentary and volcanic unit thicknesses and intensification of the diagenetic processes. At this stage, copper leaches from host rocks, and there occurs a formation of hydrotherms enriched in copper ions and other associated components of copper ores. Getting into a favorable environment (with the host rocks mostly represented by andesite porphyrites), high-grade copper hydrothermal solutions replace and recrystallize globular pyrite formed at the pre-ore stage. This process gives rise to the formation of sulfide ores mostly represented by second-generation pyrite, chalcopyrite, native ore, chalcocite, bornite, and first-generation hematite (Table 1).

Pyrite is the most abundant accessory mineral in the study area. This mineral occurs in two generations (Fig. 8). The first-generation pyrite forms in a globular shape in host rocks at the pre-ore stage which indicates reducing conditions and low temperature of its formation (Fig. 8). The second-generation pyrite mostly has a collomorphic structure and represents an aggregation of globular pyrite which formed as a result of the first-generation pyrite recrystallization. Chalcopyrite replaces mainly the first-generation pyrite and, to a lesser extent, the second-generation pyrite (Fig. 8). Bornite is one of the most abundant copper minerals and the second most abundant mineral in the study area. Bornite is observed in the form of attachment to chalcopyrite (Fig. 8).

Chalcocite is an important sulfide mineral which shows two generations. The first generation occurs mostly in veins or veinlets and replaces chalcopyrite (Fig. 8). Among the other hypogene copper minerals, it is worth noting native copper in the form of scattered nodules. Due to its softness, this mineral is a rare occurrence in polished sections (Fig. 8). In hypogenic processes, at the replacement of pyrite by copper sulfides, there is a release of iron and, therefore, a formation of the first-generation hematite. This type includes hematite nodules in rocks, and hematite rimming copper sulfides and pyrite grains.

Supergene mineralization. At this stage, there occurs a formation of the second-generation chalcocite in combination of covellite found around the chalcopyrite and bornite grains (Fig. 8).

Table 1. Stages and sequence of mineralization at copper ore deposits in the central part of the Urumieh-Dokhtar Magmatic Arc

Stage / Minerals	Pre-ore	Hypergene	Post-ore	
	Volcanism and early diagenesis	Middle – late diagenesis	Supergene	
			Sulfides	Oxides
Pyrite (I)				
Pyrite (II)				
Chalcopyrite				
Chalcocite (I)				
Chalcocite (II)				
Bornite (I)				
Bornite (II)				
Native copper				
Covellite				
Magnetite				
Hematite				
Goethite				
Malachite				
Calcite				

A general uplift of the area at the hypergene stage is caused by weathering, and alternation and decomposition of primary sulfide minerals such as chalcocite and bornite, with formation of a number of hypergenic minerals such as secondary calcite, malachite, and azurite (Table 1). The second-generation hematite, related to hypergenesis, is found on the periphery of primary magnetite or in the association with malachite. Intense weathering at the hypergenic stage leads to complete leaching of sulfide minerals as a result of which there remains malachite with a large amount of hematite (Fig. 8).

7. ORIGIN OF THE ASTANEH ORE DEPOSIT

The geochemical analysis shows that the magmatic rocks in the area are mantle-derived. Their source is considered to be the subcontinental lithospheric mantle, metasomatized by fluids detached from the subducting Neothetys oceanic plate. The study area is located between the South Ardestan and Kacho Mesghal faults which are the systems of feathering faults of the Zefreh fault zone – the Eocene-Pliocene regional fault in the central UDMA (see Fig. 1, b; 2, a). Beygi's research [Beygi et al., 2016] shows that the Zefreh and South Ardestan strike-slip fault zones are the structures intersecting the continental basement. They probably reached the lithospheric mantle and were accompanied by a rise of melts thereon. These are most likely the faults which caused decompression of the subcontinental lithosphere. Dropping tectonic stress, decompression and/or heating of the asthenosphere could cause a partial melting of the enriched mantle sources and subalkaline porphyry intrusions. Besides, the deep-seated strike-slip faults act as channels suitable not only for magma's but also for mantle fluids' migration. The afore-mentioned factors gave rise to the formation of the porphyry copper ore system and its related copper deposits in the study area.

The structural investigations of the Astaneh ore deposit show that most of the porphyry copper deposits are located along the zones of the South Ardestan strike-slip fault and at its junctions or intersections with smaller transverse faults. The results of the study allow concluding that a considerable role in formation of porphyry copper ore fields can be played by the regional ore-controlling steeply NW-dipping fault system (see Fig. 1, b).

8. CONCLUSION

Porphyry copper mineralization related the Astaneh ore deposit occurs in the southeastern Save-Ardestan ore region of the central Urumieh-Dokhtar magmatic arc. Magmatism is mainly represented by andesites, andesibasalts, basalts, and trachybasalts. These rocks are silica-rich and display characteristics of calc-alkaline magmas in island arcs related to the subduction zones. Structural investigations of all the data on tectonics of the study area show that most of the porphyry copper ore fields and ore deposits are confined to the northwest-striking fault zones. The South Ardestan fault, striking northwest and intersecting the continental basement structures, forms active permeable zones providing conditions for upwelling of magmas and fluids, i.e. for the formation of porphyry copper ore fields.

Considering the secondary wall rock alternations of copper ores, represented by large-scale propylitic aureoles with sericite, chlorite, epidote, carbonate and iron oxide mineralization, it can be concluded that during magmatic intrusions the copper-bearing post-magmatic fluids penetrated the volcanic units and favored further heating and

hydrothermal-metasomatic alternation of surrounding rocks, especially in permeable fault zones.

9. CONTRIBUTION OF THE AUTHORS

The first author contributed 50 %, the other authors contributed equally to the analysis and preparing this article. All authors read and approved the final manuscript.

10. DISCLOSURE

The authors declare that they have no conflicts of interest relevant to this manuscript.

11. REFERENCES

Aftabi A., Atapour H., 2000. Regional Aspects of Shoshonitic Volcanism in Iran. Episodes 23 (2), 119–125.

Afzal P., Alghalandis Y.F., Moarefvand P., Omran N.R., Haroni H.A., 2012. Application of Power-Spectrum–Volume Fractal Method for Detecting Hypogene, Supergene Enrichment, Leached and Barren Zones in Kahang Cu Porphyry Deposit, Central Iran. Journal of Geochemical Exploration 112, 131–138. https://doi.org/10.1016/j.gexplo.2011.08.002.

Ageev A., Egorov A., Krikun N., 2020. The Principal Characterized Features of Earth's Crust within Regional Strike-Slip Zones. In: V. Litvinenko (Ed.), Advances in Raw Material Industries for Sustainable Development Goals. Proceedings of the XII Russian-German Raw Materials Conference (November 27–29, 2019, Saint Petersburg) Taylor & Francis, London, p. 78–83. https://doi.org/10.1201/9781003164395-11.

Aghazadeh M., Hou Z., Badrzadeh Z., Zhou L., 2015. Temporal–Spatial Distribution and Tectonic Setting of Porphyry Copper Deposits in Iran: Constraints from Zircon U-Pb and Molybdenite Re-Os Geochronology. Ore Geology Reviews 70, 385–406. https://doi.org/10.1016/j.oregeorev.2015.03.003.

Alaminia Z., Tadayon M., Finger F., Lentz D.R., Waitzinger M., 2020. Analysis of the Infiltrative Metasomatic Relationships Controlling Skarn Mineralization at the Abbas-Abad Fe-Cu Deposit, Isfahan, North Zefreh Fault, Central Iran. Ore Geology Reviews 117, 103321. https://doi.org/10.1016/j.oregeorev.2020.103321.

Alavi M., 1991. Sedimentary and Structural Characteristics of the Paleo-Tethys Remnants in Northeastern Iran. Geological Society of America Bulletin 103 (8), 983–992. https://doi.org/10.1130/0016-7606(1991)103%3C0983:SASCOT%3E2.3.CO;2.

Allen M., Jackson J., Walker R., 2004. Late Cenozoic Reorganization of the Arabia-Eurasia Collision and the Comparison of Short-Term and Long-Term Deformation Rates. Tectonics 23 (2), 1–16. https://doi.org/10.1029/2003TC001530.

Arshamov Ya.K., 2013. Typical Textures and Geological and Genetic Traits of Porphyry Copper Deposits. Bulletin of KazNTU 97 (3), 22–28 (in Russian) [Аршамов Я.К. Типовые модели и геолого-генетические особенности медно-порфировых месторождений // Вестник КазНТУ. 2013. Т. 97. № 3. С. 22–28].

Atapour H., Aftabi A., 2007. The Geochemistry of Gossans Associated with Sarcheshmeh Porphyry Copper Deposit, Rafsanjan, Kerman, Iran: Implications for Exploration and the Environment. Journal of Geochemical Exploration 93 (1), 47–65. https://doi.org/10.1016/j.gexplo.2006.07.007.

Babazadeh S., Ghorbani M.R., Bröcker M., D'Antonio M., Cottle J., Gebbing T., Carmine Mazzeo F., Ahmadi P., 2017. Late Oligocene–Miocene Mantle Upwelling and Interaction Inferred from Mantle Signatures in Gabbroic to Granitic Rocks from the Urumieh–Dokhtar Arc, South Ardestan, Iran. International Geology Review 59 (12), 1590–1608. https://doi.org/10.1080/00206814.2017.1286613.

Berberian F., Berberian M., 1981. Tectono-Plutonic Episodes in Iran. In: H.K. Gupta, F.M. Delany (Eds), Zagros, Hindu Kush, Himalaya: Geodynamic Evolution. Vol. 3. American Geophysical Union, Washington, p. 5–32. DOI:10.1029/GD003p0005.

Beygi S., Nadimi A., Safaei H., 2016. Tectonic History of Seismogenic Fault Structures in Central Iran. Journal of Geosciences 61 (2), 127–144. https://doi.org/10.3190/JGEOSCI.212.

Beygi S., Talovina I.V., Ilalova R.K., Durjagina A.M., 2018a. Regional Geological Structure of the Volcanogenic-Plutonic Belt of Urumyedohtar in the Central Iran. Mining Informational and Analytical Bulletin S29, 17–24 (in Russian) [Бейги С., Таловина И.В., Илалова Р.К., Дурягина А.М. Региональное геологическое строение вулканогенно-плутонического пояса Уромие-Дохтар в Центральном Иране // Горный информационно-аналитический бюллетень. 2018. № S29. С. 17–24]. https://doi.org/10.25018/0236-1493-2018-17-24.

Beygi S., Talovina I.V., Krikun N.S., 2021a. Evaluation of Neotectonic Activity within the Urumieh-Dokhtar Volcanic Arc (Iran) Based on the Calculation of Morphotectonic Indices. Bulletin of Moscow University. Series 5. Geography, 3, 64–76 (in Russian) [Бейги С., Таловина И.В., Крикун Н.С. Оценка неотектонической активности в центральной части вулканической дуги Уромие-Дохтар на основе расчета морфотектонических индексов // Вестник Московского университета. Серия 5. География. 2021. № 3. С. 64–76].

Beygi S., Talovina I.V., Tadayon M., Nadimi A., 2018b. Tectonics and Mineralization in the Urumieh-Dokhtar Magmatic Arc of Iran. In: V. Litvinenko (Ed.), Topical Issues of Rational Use of Natural Resources. Proceedings of the XIV International Forum-Contest of Young Researchers (April 18–20, 2018, Saint Petersburg). CRC Press, USA, p. 9–16.

Beygi S., Talovina I.V., Tadayon M., Pour A.B., 2021b. Alteration and Structural Features Mapping in Kacho-Mesqal Zone, Central Iran Using Aster Remote Sensing Data for Porphyry Copper Exploration. International Journal of Image and Data Fusion 12 (2), 155–175. https://doi.org/10.1080/19479832.2020.1838628.

Chiu H.Y., Chung S.L., Zarrinkoub M.H., Melkonyan R., Pang K.N., Lee H.Y., Wang K.L., Mohammadi S.S., Khatib M.M., 2017. Zircon Hf Isotopic Constraints on Magmatic and Tectonic Evolution in Iran: Implications for Crustal Growth in the Tethyan Orogenic Belt. Journal of Asian Earth Sciences

145, 652–669. https://doi.org/10.1016/j.jseaes.2017.06.011.

Frost B.R., Frost C.D., 1969. A Geochemical Classification for Feldspathic Igneous Rocks. Journal of Petrology 49 (11), 1955–1969. https://doi.org/10.1093/petrology/egn054.

Gzovsky M.V., 1975. Fundamentals of Tectonophysics. Nauka, Moscow, 536 p. (in Russian) [Гзовский М.В. Основы тектонофизики. М.: Наука, 1975. 536 с.].

Hansen J., Skjerlie K.P., Pedersen R.B., De La Rosa J., 2002. Crustal Melting in the Lower Parts of Island Arcs: An Example from the Bremanger Granitoid Complex, West Norwegian Caledonides. Contributions to Mineralogy and Petrology 143, 316–335. https://doi.org/10.1007/s00410-001-0342-5.

Krivtsov A.I., 1983. Fundamentals of Geological Prediction and Search for Porphyry Copper Deposits. Nedra, Moscow, 256 p. (in Russian) [Кривцов А.И. Геологические основы прогнозирования и поисков медно-порфировых месторождений. М: Недра, 1983. 256 с.].

Krivtsov A.I., Migachev I.F., Popov V.S., 1986. Porphyry Copper Deposits of the World. Nedra, Moscow, 236 p. (in Russian) [Кривцов А.И., Мигачев И.Ф., Попов В.С. Медно-порфировые месторождения мира. М.: Недра, 1986. 236 с.].

Le Bas M.J., Streckeisen A.L., 1991. The IUGS Systematics of Igneous Rocks. Journal of the Geological Society 148 (5), 825–833. https://doi.org/10.1144/gsjgs.148.5.0825.

Nogol-Sadat M.A.A., 1985. Transpressional Structures in Iran. Results of Structural Analysis of Qom Region. Geological Surveying of Iran, Report 55.

Parfenov L.M., Berzin N.A., Khanchuk A.I., Badarch G., Belichenko V.G., Bulgatov A.N., Dril S.I., Kirillova G.L. et al., 2003. Model of the Formation of Orogenic Belts in Central and North-East Asia. Pacific Geology 22 (6), 7–41 (in Russian) [Парфенов Л.М., Берзин Н.А., Ханчук А.И., Бадарч Г., Беличенко В.Г., Булгатов А.Н., Дриль С.И., Кириллова Г.Л. и др. Модель формирования орогенных поясов Центральной и Северо-Восточной Азии // Тихоокеанская геология. 2003. Т. 22. № 6. С. 7–41].

Pearce J.A., 1983. Role of Subcontinental Lithosphere in Magma Genesis at Active Continental Margins. In: C.J. Hawkesworth, M.J. Norry (Eds), Continental Basalts and Mantle Xenoliths. Shiva, Nantwich, p. 230–249.

Richards J.P., 2005. Cumulative Factors in the Generation of Giant Calc-Alkaline Porphyry Cu Deposits. In: T.M. Porter (Ed.), Super Porphyry Copper & Gold Deposits: A Global Perspective. Vol. 1. PGC Publishing, Adelaide, 7–25.

Richards J.P., Sholeh A., 2016. The Tethyan Tectonic History and Cu-Au Metallogeny of Iran. In: J.P. Richards (Ed.), Tectonics and Metallogeny of the Tethyan Orogenic Belt. Society of Economic Geologists Special Publication 19, 193–212. DOI:10.5382/SP.19.07.

Richards J.P., Spell T., Rameh E., Razique A., Fletcher T., 2012. High Sr/Y Magmas Reflect Arc Maturity, High Magmatic Water Content, and Porphyry Cu±Mo±Au Potential: Examples from the Tethyan Arcs of Central and Eastern Iran and Western Pakistan. Economic Geology 107 (2), 295–332. https://doi.org/10.2113/econgeo.107.2.295.

Salvini F., 1998. Daisy 5.38 Software: The Structural Data Integrated System Analyser. Roma Tre University.

Sarjoughian F., Kananian A., 2017. Zircon U-Pb Geochronology and Emplacement History of Intrusive Rocks in the Ardestan Section, Central Iran. Geologica Acta 15 (1), 25–36. DOI:10.1344/GeologicaActa2017.15.1.3.

Sayari M., Sharifi M., Manesh S.M.T., Ahmadian J., 2015. Evaluating Physicochemical Conditions of Miocene–Pliocene Volcanic Rocks in the Middle Part of the Urumieh-Dokhtar Magmatic Arc. Arabian Journal of Geosciences 8, 9501–9516. https://doi.org/10.1007/s12517-015-1856-x.

Shafiei B., Haschke M., Shahabpour J., 2009. Recycling of Orogenic Arc Crust Triggers Porphyry Cu Mineralization in Kerman Cenozoic Arc Rocks, South-Eastern Iran. Mineralium Deposita 44, 265–283. https://doi.org/10.1007/s00126-008-0216-0.

Shahabpour J., 2005. Tectonic Evolution of the Orogenic Belt in the Region Located between Kerman and Neyriz. Journal of Asian Earth Sciences 24 (4), 405–417. https://doi.org/10.1016/j.jseaes.2003.11.007.

Sillitoe R.H., 2010. Porphyry Copper Systems. Economic Geology 105 (1), 3–41. https://doi.org/10.2113/gsecongeo.105.1.3.

Zarasvandi A., Liaghat S., Zentilli M., 2005. Geology of the Darreh-Zerreshk and Ali-Abad Porphyry Copper Deposits, Central Iran. International Geology Review 47 (6), 620–646. https://doi.org/10.2747/0020-6814.47.6.620.